Electronic Supplementary Material (ESI) for Soft Matter.

Supplemental Information – Microstructure and elasticity of dilute gels of colloidal discoids

Peng-Kai Kao[†], Michael J. Solomon[†,*], and Mahesh Ganesan[†,*]

[†]Department of Chemical Engineering, University of Michigan, Ann Arbor, Michigan

***Corresponding Authors:**

Prof. Michael J. Solomon

Address: North Campus Research Complex, Building 10 – A151, 2800 Plymouth Road, Ann Arbor, MI 48109

Phone: 734-764-3119

Email: mjsolo@umich.edu

Dr. Mahesh Ganesan

Address: North Campus Research Complex, Building 20 –106W, 2800 Plymouth Road, Ann Arbor, MI 48109

Phone: 734-546-0210

Email: maheshg@umich.edu

Supplemental Figures

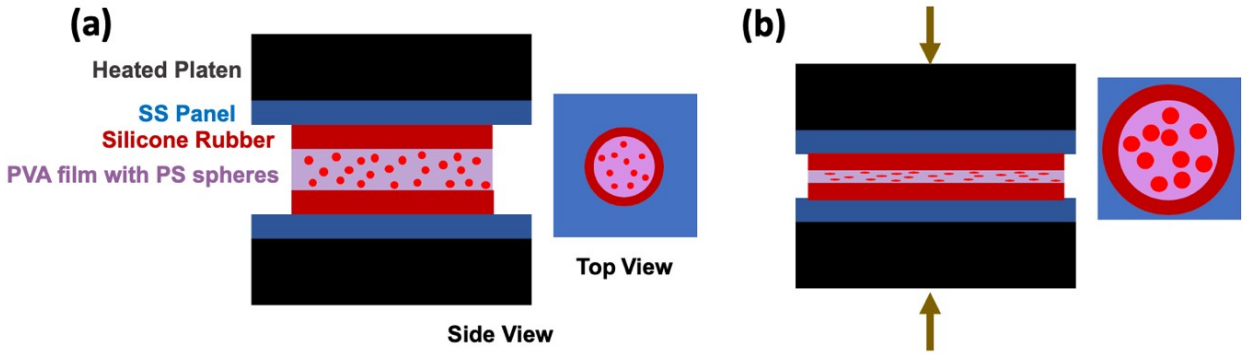

Figure S1. Schematic of discoid synthesis process. **(a)** Seed polystyrene (PS) microspheres, embedded in a poly(vinyl alcohol) (PVA) film, are sandwiched between silicone rubber carriers (50A durometer, 0.5mm thick) and placed in between 1 mm thick stainless-steel (SS) panels (152 mm x 152 mm) housed inside a heated plate press. **(b)** Uniaxial compression leads to equi-biaxial deformation of the layers resulting in oblate discoids. The method is adapted from Ahn et al[1].

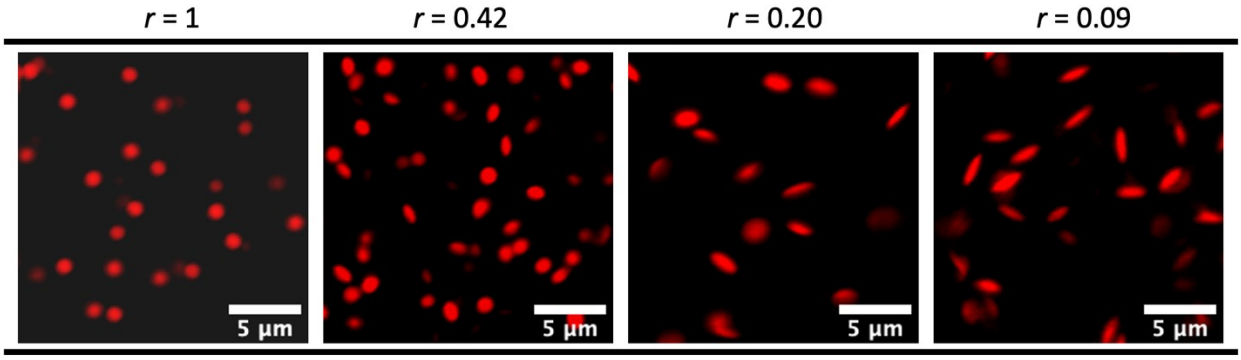

Figure S2. Confocal micrograph of dilute suspension of spheres (r = 1) and synthesized discoids (r = 0.42, 0.20 and 0.09). The dilute discoidal suspensions are well-dispersed prior to gelation.

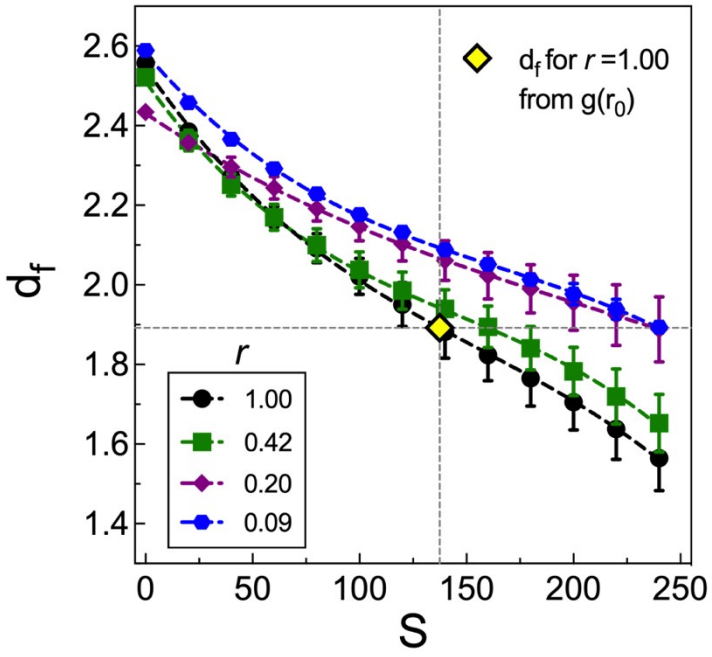

Figure S3. Dependence of box-counting fractal dimension, ^{d_f}, on image threshold parameter, S, measured from confocal image volumes of colloidal gels consisting of spheres (r = 1) and discoids (r = 0.42, 0.20 and 0.09). The optimal threshold derived from fitting, following Thill and co-workers[2], as described in the main text, for each aspect ratio, are S = 136, 144, 152 and 141 for r = 1, 0.42, 0.20 and 0.09 respectively. The ^{d_f} for sphere gels (r = 1) obtained from its radial distribution function, $^{g(r_0)}$, (SI Figure S4) is indicated by the horizontal dashed line and marked as solid diamond on the curve corresponding to r = 1; the corresponding threshold, S = 138, is indicated by the vertical dashed line.

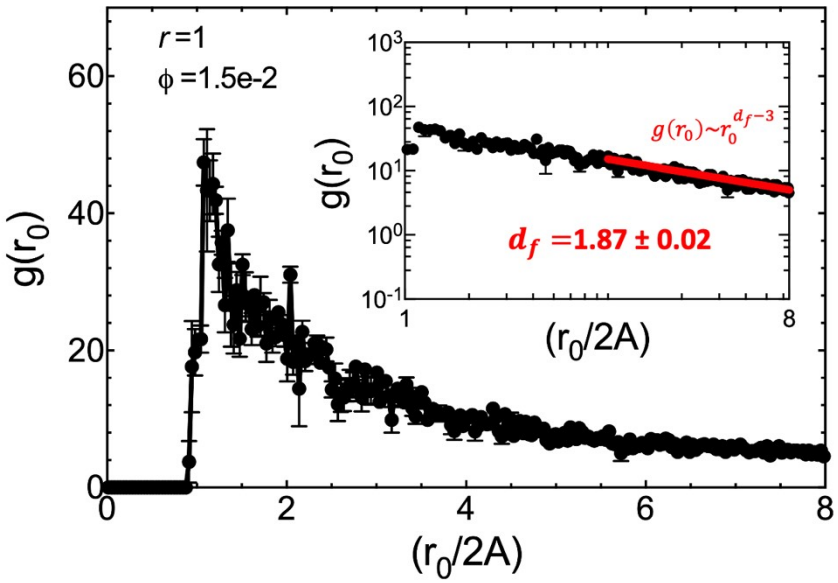

Figure S4. Radial distribution function, $g(r_0)$ of sphere gels (r =1). $g(r_0)$ describes the average number of particles at a distance r_0 from a basis particle, relative to that of an ideal gas. In the fractal regime, the functional dependence of $g(r_0)$ is given as: $g(r_0) \sim r_0^{d_f - 3}$. As shown in the inset plot, we observe this fractal scaling for $r_0/2A > 3$, which is consistent with that reported by others [4]. The solid line is a fit to the data as per the above equation and the resulting d_f is mentioned in the inset. The particle volume fraction is $\phi = 0.015$ and $[MgCl_2] = 10mM$.

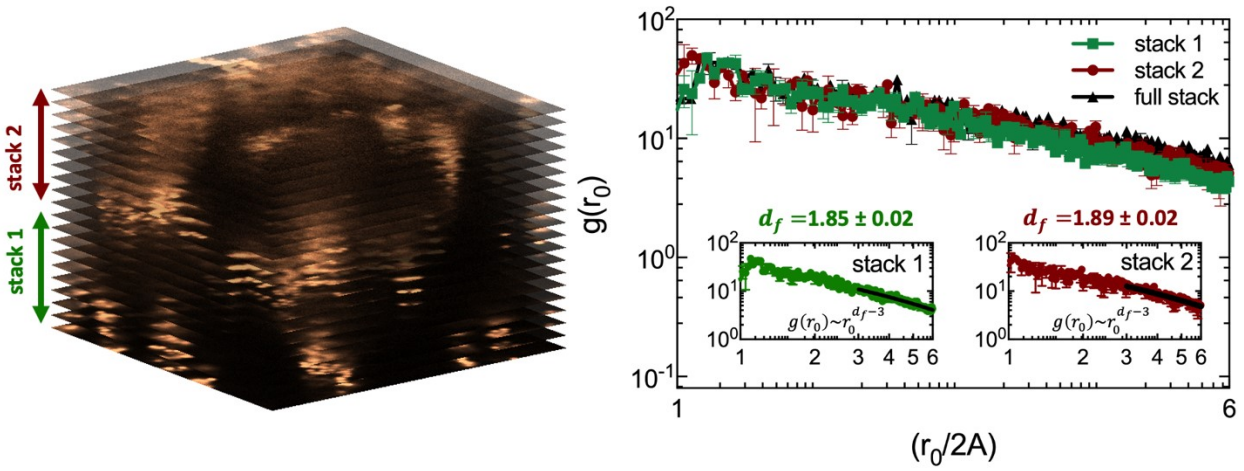

Figure S5. Wall effects on the analysis of gel fractal dimension. **(left)** The confocal image volume of a sphere colloidal gel is divided into equal half-stacks, stack 1 and stack 2, each of height ~ 8 microns. **(right)** The radial distribution function, $g(r_0)$ of stack 1 and stack 2 compared to that of the full stack (the full stack $g(r_0)$ is from SI Figure S4). For $r_0/2A > 3$, a fractal scaling is observed for both the stacks and the inset plots shows the fits of the data to: $g(r_0) \sim r_0^{d_f - 3}$. The resulting fractal dimensions, d_f for each stack are statistically similar with that obtained for the full stack from SI Figure S4 (one-way ANOVA yields $p = 0.7025$). The particle volume fraction is $\phi = 0.015$ and [$MgCl_2$] = 10mM.

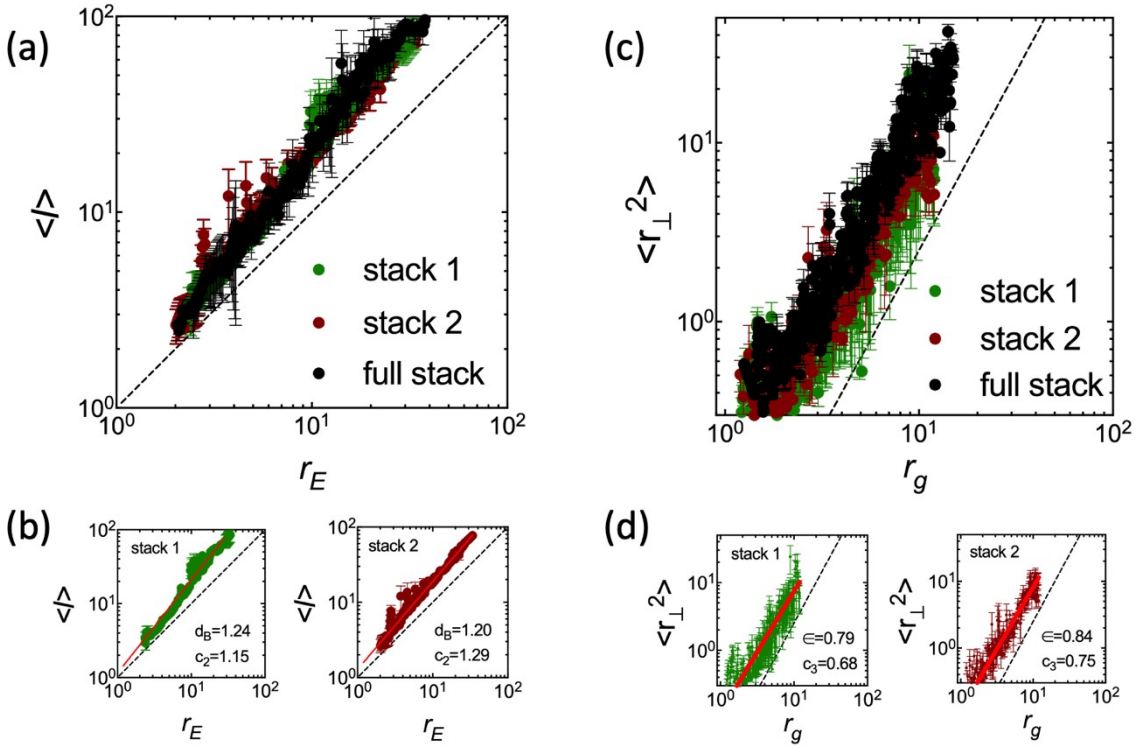

Figure S6. Results of skeletonization image analysis applied to two half-stacks of a sphere gel (c.f. SI Figure S5) and compared to that obtained for the full stack image volume (from Figure 5 of the main text). **(a)** Log-log plot of $\langle l \rangle$ versus r_E for stack 1 and stack 2 compared to that of the full stack (the full stack results are from Figure 5, main text). **(b)** Power-law fits of the data to $\langle l \rangle = c_2 r_E^{d_B}$. The resulting values for the backbone dimension, d_B for stack 1 ($d_B = 1.24 \pm 0.04$) and stack 2 ($d_B = 1.20 \pm 0.02$) are statistically similar to that obtained for the full image volume ($d_B = 1.26 \pm 0.03$). The p-value from a one-way ANOVA is $p = 0.4085$. **(c)** Log-log plot of $\langle r_\perp^2 \rangle$ versus r_g for stack 1 and stack 2 compared to that of the full stack (the full stack results are from Figure 5, main text). **(d)** Power-law fits of the data to $\langle r_\perp^2 \rangle = c_3 r_g^{2\epsilon}$. The resulting values for the backbone anisotropy, ϵ for stack 1 ($\epsilon = 0.79 \pm 0.03$) and stack 2 ($\epsilon = 0.84 \pm 0.01$) are statistically similar to that obtained for the full image volume ($\epsilon = 0.80 \pm 0.02$). A one-way ANOVA produces $p = 0.2621$.

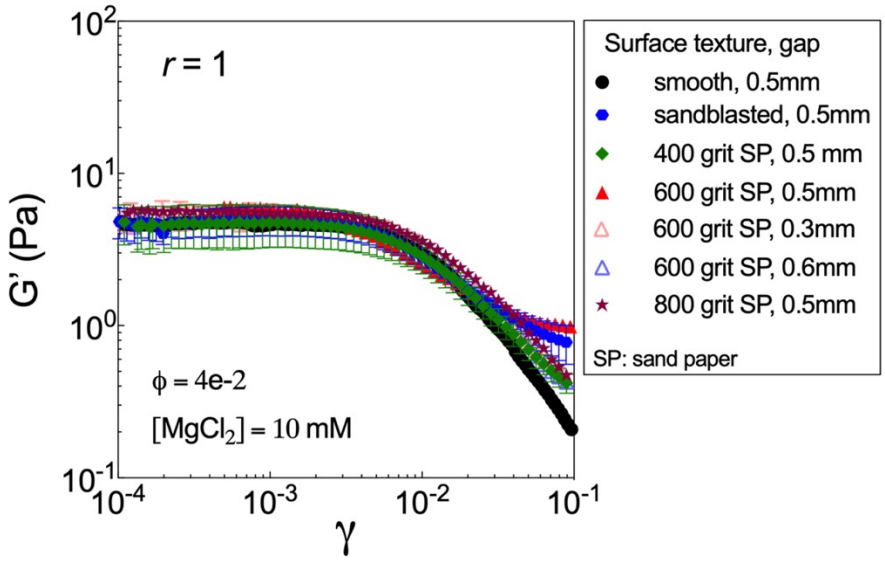

Figure S7. Checking for slip in oscillatory shear rheology. Storage modulus (G') as a function of strain amplitude (γ) for a sphere gel ($r = 1$) measured using a 40mm diameter parallel plate geometry having different surface textures and at different measurement gaps. When testing with sandpaper, the sandpaper was attached to both the bottom and top bounding surfaces. The relative standard deviation in the linear storage modulus is less than 10% indicating the upper bound on any potential effects of wall-slip. Here, the particle volume fraction is $\phi = 0.04$ and $[MgCl_2]$ = 10mM.

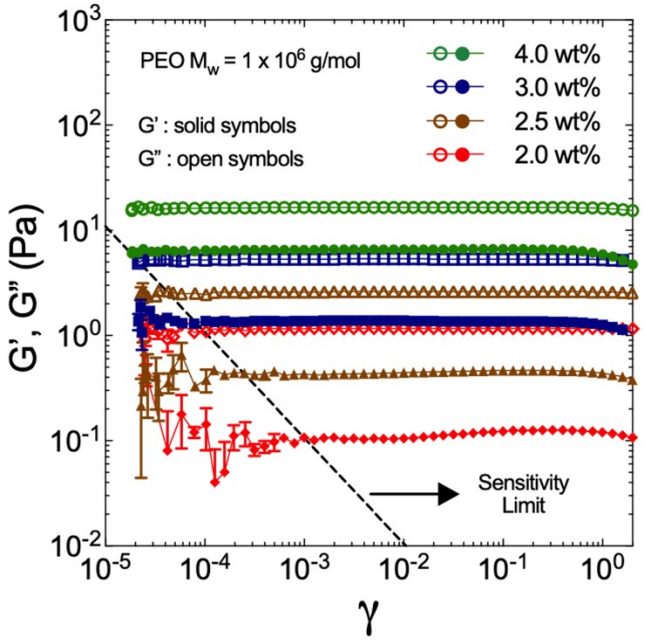

Figure S8. The lower stress limit of the rheometer used in this study was estimated from oscillatory amplitude sweep measurements of polyethylene oxide (PEO) solutions of different concentrations (2.0, 2.5, 3.0 and 4.0 wt %). Minimum shear amplitudes at which the measured storage (G') and loss (G'') moduli were consistent – having a variation of less than 2.5% with increasing shear strain – define the lower stress limit of the rheometer, marked here as the dashed line.

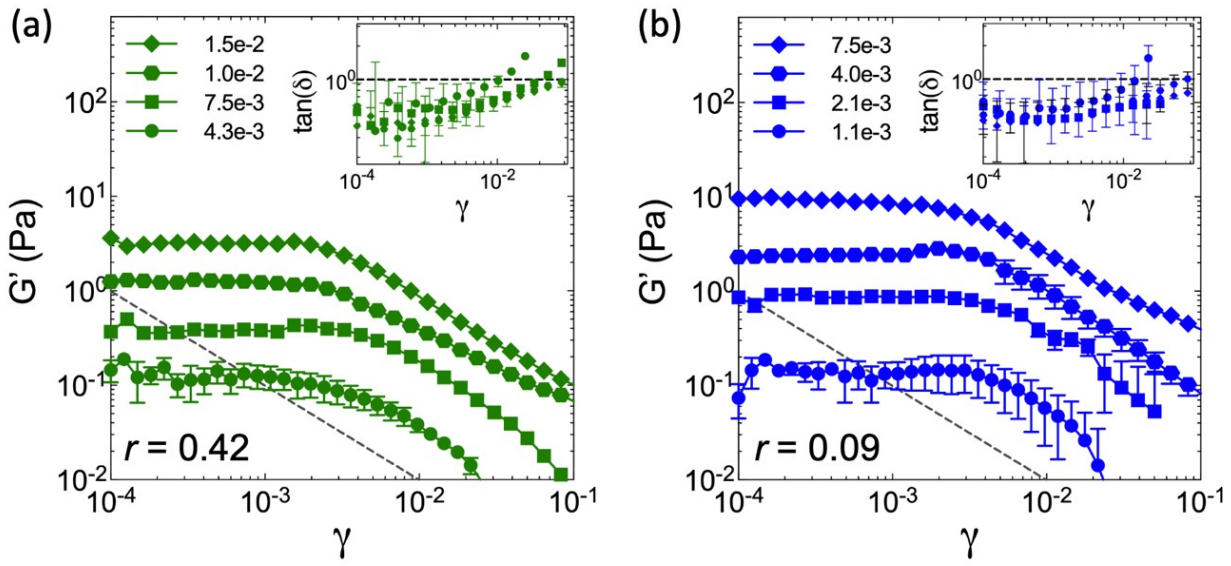

Figure S9. Storage modulus, G' and (inset) tan(δ) as a function of strain amplitude, γ for colloidal gels made from discoids of aspect ratio (a) r = 0.42 and (b) r = 0.09. The oscillation frequency is 1 rad/s. The dashed line indicates the instrument sensitivity limits. The concentration of $MgCl_2$ is 10mM.

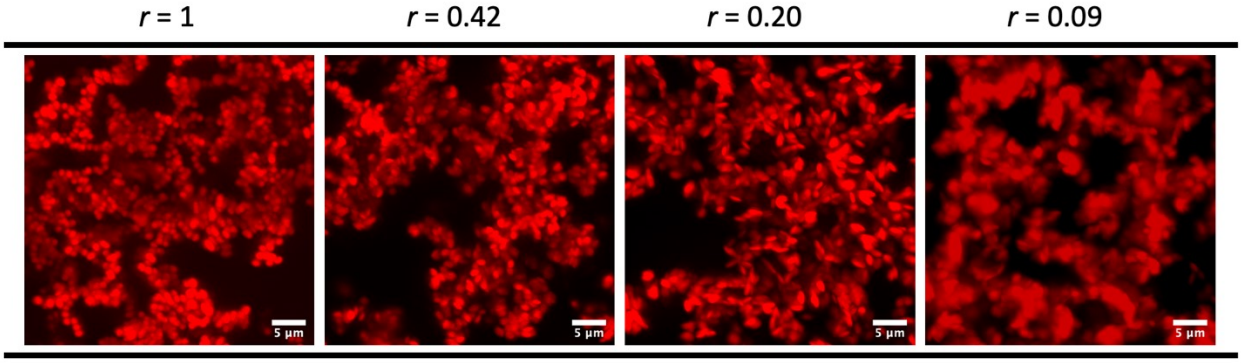

Figure S10. Confocal projections for skeletonization analysis. Real space confocal maximum projections (Δz = 20μm) of colloidal gels consisting of spheres (r = 1) and discoids (r = 0.42, 0.20 and 0.09) whose iso-surface rendering and extracted skeletons are shown in Figure 5(a) of the main manuscript. Here, ϕ = 0.015 and [$MgCl_2$] = 10mM.

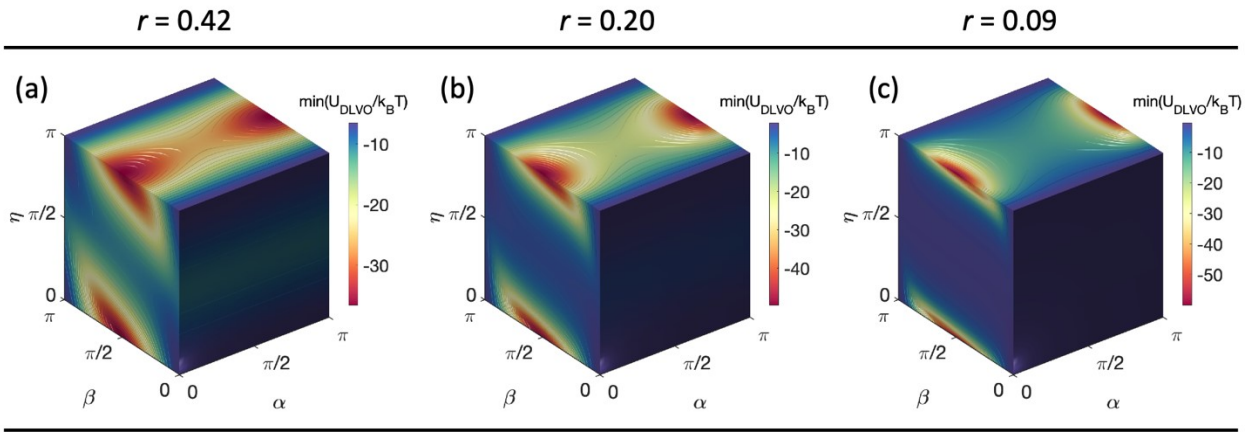

Figure S11. Potential energy for interacting discoid pairs. Strength of the DLVO interparticle potential energy (U_{DLVO}) as a function of relative orientation for a pair of discoids with aspect ratio (a) r = 0.42, (b) r = 0.20 and (c) r = 0.09. The DLVO potential here is a sum of nonretarded van der Waal's attraction and electrostatic repulsion potential. The expressions for calculating the orientation dependent DLVO potentials for discoids are given in Schiller et al[5]. They describe the mutual orientation of a pair of discoids in terms of angles α,β, and η. Here, α denotes the angle of relative orientation of the two coordinate systems that define the principal radii of curvature of the two particles, β is the polar angle relative to the major axis and η is the angle enclosed by their axes of revolution. This figure highlights the range of potential energies possible due to interaction anisotropy accorded by the discoidal particle shape. The energetically favorable F-F configuration discussed in the main text corresponds to (α,β,η) = (0, π/2, 0). We find that the F-F bond energy increases with increasing discoid anisotropy (decreasing r). The E-E, E-F and ExE configurations shown in Figure 6(a)-(b) of the main text, respectively correspond to (α,β,η) = (0,0,0), (0,0, π/2) and (π/2, π/2,0). To compute the bond spring constant, we average over all the possible potential states plotted in (a), (b) and (c) by considering the probability for sampling the different orientations to satisfy the Boltzmann distribution. Here, the potential energy is normalized by k_BT, where k_B = Boltzmann constant and T is the temperature.

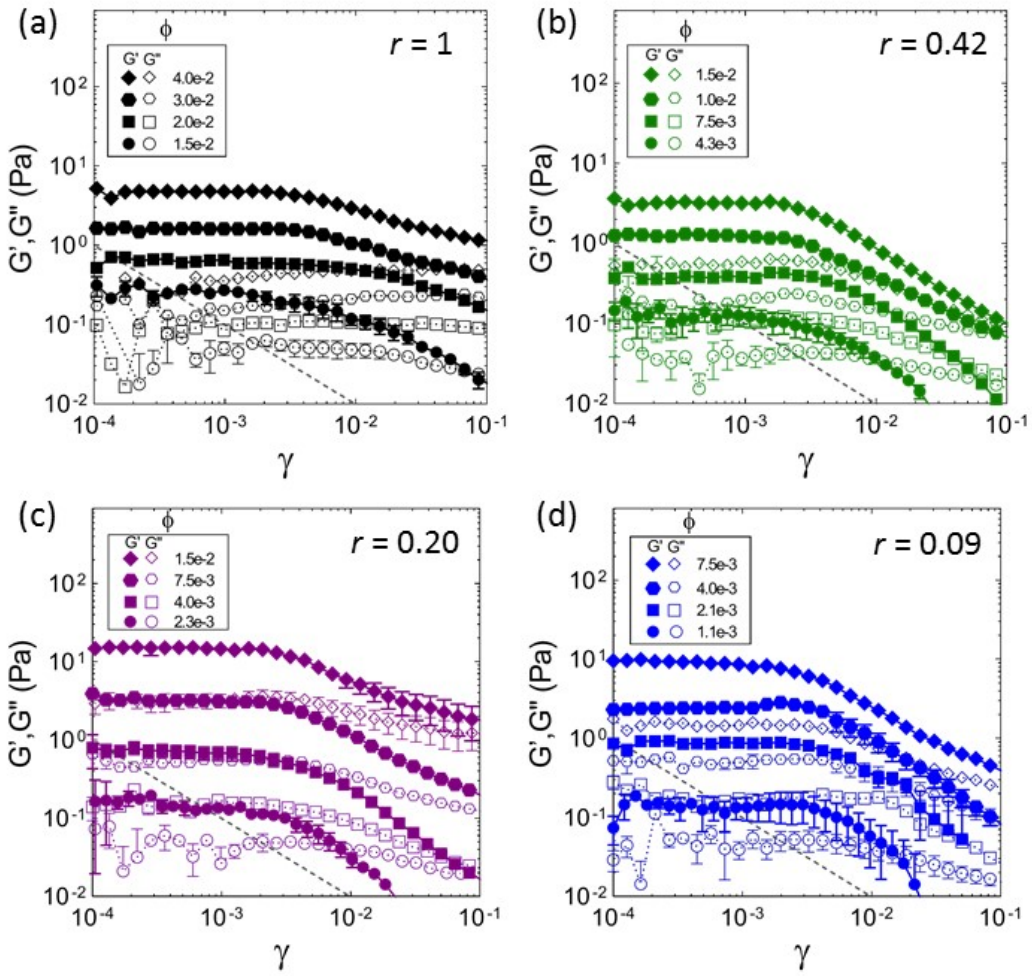

Figure S12. Storage (G', solid symbols) and loss (G'', open symbols) modulus as a function of strain amplitude, γ for colloidal gels made from particles of aspect ratio (a) r = 1, (b) r = 0.42, (c) r = 0.20 and (d) r = 0.09. The oscillation frequency is 1 rad/s. The dashed line indicates the instrument sensitivity limits. The concentration of $MgCl_2$ is 10mM. The rapid decrease in both G' and G''at high strain amplitudes (> 0.003) represents a progressive yielding of the gel and the $G' - G''$ cross-over indicates a fluidization transition.

References

1 S. J. Ahn, K. H. Ahn and S. J. Lee, *Colloid Polym. Sci.*, 2016, **294**, 859–867.

2 A. Thill, S. Veerapaneni, B. Simon, M. Wiesner, J. Y. Bottero and D. Snidaro, *J. Colloid Interface Sci.*, 1998, **204**, 357–362.

3 K. T. Saud, M. Ganesan and M. J. Solomon, *J. Rheol.*, 2021, **65**, 225–239.

4 M. Lattuada, H. Wu, A. Hasmy and M. Morbidelli, *Langmuir*, 2003, **19**, 6312–6316.

5 P. Schiller, S. Krüger, M. Wahab and H.-J. Mögel, *Langmuir*, 2011, **27**, 10429–10437.